Biotechnology and Bioprocess Engineering 20: 576-584 (2015)
DOI 10.1007/s12257-014-0397-6

RESEARCH PAPER

Growth-dependent Surface Characteristics of *Hansenula polymorpha*: Implications for Expanded Bed Adsorption Chromatography

Nadia Naz, Roy N. Dsouza, Vikas Yelemane, Rami Reddy Vennapusa, Martin Kangwa, and Marcelo Fernández-Lahore

Received: 5 June 2014 / Revised: 24 February 2015 / Accepted: 15 March 2015

Abstract The cell surface characteristics of a methylotrophic wild-type strain of yeast, *Hansenula polymorpha*, was investigated at different growth stages (early log, late log, stationary and death) of the biomass under different conditions (low and high salt in intact and disrupted forms) using extended DLVO theory. Biomass was characterized by contact angle measurements as well as zeta potential determinations. These measurements were used to describe the hydrophobic, polar, and electrostatic behavior of the biomass in its growth stages. Consequently, interaction free energy *vs.* distance profiles of the biomass with anion-exchange and HIC adsorbents were conveniently generated. A strong interaction was calculated between cells and the adsorbents in the stationary and death phases of the biomass illustrated by the striking correlation between theoretical predictions and biomass deposition experiments. The physico-chemical properties of biomass in different growth phases have important implications for expanded bed adsorption chromatography, where unfavorable biomass-adsorbent interactions adversely affect process efficiency.

Keywords: expanded bed adsorption, chromatography, extended DLVO theory, surface energetics, cell adhesion, hydrophobic interaction, ion exchange, microbial growth

Nadia Naz, Roy N. Dsouza, Vikas Yelemane, Martin Kangwa, Marcelo Fernández-Lahore*
Downstream Bioprocessing Laboratory, School of Engineering and Science, Jacobs University, Campus Ring 1, D-28759 Bremen, Germany
Tel: +49-421-200-3239; Fax: +49-421-200-3600
E-mail: m.fernandez-lahore@jacobs-university.de

Rami Reddy Vennapusa
Manufacturing Technologies Laboratory, Shantha Biotechnics (A Sanofi Company), Hyderabad 501-401, India

1. Introduction

The product portfolio of bioprocess industries is constantly increasing and ranges from food to medical applications. Especially in the pharmaceutical industry, emerging therapeutic bioproducts, such as enzymes, monoclonal antibodies, or virus-like particles, offer powerful and effective ways to combat several diseases [1,2]. The consequent growth in demand for these products has exposed several bottlenecks in their manufacture and purification [3]. While upstream processes have undergone intensive advancements in terms of process yield and variety, corresponding downstream processing technologies have struggled to keep up. More importantly, these downstream operations consist of several steps and can account for up to 80% of the total production cost [4,5]. The novelty of the numerous bioproducts currently under development, coupled with their considerable demand poses a challenge that needs to be commensurately addressed by economical and efficient processing and purification technologies [6]. Expanded bed adsorption (EBA) is a primary recovery technology, which offers process integration and intensification by simultaneously combining clarification, capture, and concentration within a single step directly from crude cell feedstock [3,7,8]. It has previously been used to purify numerous bioproducts including recombinant annexin V from *Escherichia coli* [9], cutinase from *Saccharomyces cerevisiae* [10], mouse endostatin and β-glucosidase from *Pichia pastoris*, recombinant protein and monoclonal antibodies from Chinese hamster ovary cells [11,12]. Furthermore, process times can be reduced by up to 50% [13], while realizing economic savings of up to 70% [14].

The widespread adoption of EBA technology, however, has been limited by caveats related to its performance with certain crude feedstock, especially where unfavorable

adsorbent-biomass interactions led to adsorbent aggregation, reduced product binding, poor hydrodynamics, and ultimately, bed collapse [15]. The effects of the biomass-adsorbent interactions of different biomass types and their homogenates on the chromatographic performance of a number of commercial adsorbents (Streamline DEAE, SP, phenyl, and chelating matrices) have been studied extensively [15-20]. However, it is crucial to understand these interactions from a fundamental perspective. *H. polymorpha* like other methylotrophic yeast strains has a rigid bilayer cell wall, mainly composed of mannoproteins linked convalently to glucans, to lesser extent chitin, and is located outside of the plasma membrane [21-24]. This cell wall/ surface undergo rearrangements during cell growth and this physicochemical/ or specific molecular character of the cell surface composition can be key to better understand the interaction to solid supports [25,26]. We have previously demonstrated the application of colloid theory methods, namely, extended *Derjaguin, Landau, Verwey* and *Overbeek* (xDLVO) theory, in successfully explaining these interactions [27]. This theory involves a complete thermodynamic (*via* contact angle measurements) and electrostatic (*via* zeta potential measurements) characterization of the interacting surfaces (biomass/ cell wall as well as adsorbent) at different solution conditions, *i.e.*, ionic strength, electrolyte composition, and pH [17,28], in order to reveal distance-dependent interaction energy profiles between the two surfaces.

In this study, we investigate the progressive changes in cell surface properties of *H. polymorpha* during its different growth phases (early log, late log, stationary, and death) and their corresponding interactions with anion-exchange (Streamline DEAE) and hydrophobic interaction (Streamline phenyl) adsorbents in different solution conditions. Understanding the ability of cell surfaces to effectively interact with adsorbents can positively help in defining conditions suitable for application in industrial downstream bioprocessing of therapeutics and several other biological processes like biobeneficiation, bioleaching, bioremediation and biodeterioration [29,30]. We have additionally supplemented theoretically calculated interaction energies with experimental cell partition indices (CTI), thereby establishing an important link between the nanoscale (*via* xDLVO calculations) and the process scale (*via* CTI experiments). To our knowledge, this is the first reported instance of cell surface characterization to different growth phases.

2. Material and Methods

2.1. Chemicals and reagents

1-Bromonaphtalene and formamide were obtained from Fluka (Buchs, Switzerland). Buffer salts, glycerol, yeast culture media components, such as yeast extract, peptone, D-glucose, and agar, were obtained from AppliChem (Darmstadt, Germany). Milli-Q water (0.055 mS/cm) was used for all experiments.

2.2. Instrumentation

Chromatographic adsorbents (Streamline DEAE and Phenyl Sepharose CL-4B), C-10 [31] columns, and the ÄKTA explorer system were obtained from GE Healthcare (Munich, Germany). The goniometric system (OCA 20) was obtained from DataPhysics Instruments (Filderstadt, Germany). Zeta potentials were measured with a Zetasizer Nano ZS from Malvern Instruments (Worcestershire, UK).

2.3. Biomass cultivation and harvesting

Methylotrophic wild-type *H. polymorpha* was grown on plates containing yeast extract-peptone-dextrose (YPD) agar medium (yeast extract 10 g/L, peptone 20 g/L, dextrose 20 g/L and agar 20 g/L). YPD medium without agar was used for liquid culture. The culture was incubated at 37°C under shaking (*ca.* 220 RPM) till the end of growth. Growth and viability [32] was monitored at two-hour and ten-hour intervals by optical density measurements at 600 nm and by trypan blue followed by microscopic counting (Fig. 1), respectively. Cells were harvested by centrifugation at 1,800 *g*, washed thrice with water in order to remove any remaining contaminants, and finally re-suspended in 20 mM phosphate buffer at pH 7.

2.4. Contact angle measurements

Cell lawns were prepared for contact angle measurements in a similar fashion as reported previously [27,33]. Cell pellets were suspended in 20 mM phosphate buffer at pH 7 to make a final concentration (wet cell weight) of 10% (w/v). This solution was then deposited on solidified agar plates (glycerol 100 g/L and agar 20 g/L), which were then incubated for 24 h at room temperature. These agar plates were cut in small squares for contact angle measurements. Contact angles were measured by the sessile drop technique at room temperature in dust free environments using three different liquids with known surface tension parameters, *i.e.*, water, formamide, and 1-bromonaphthalene. All measurements were performed in triplicate using intact as well as disrupted cells in low salt (20 mM phosphate buffer at pH 7) and high salt (1 M ammonium sulfate in 20 mM phosphate buffer at pH 7) conditions.

2.5. Zeta potential measurements

Intact or disrupted cells in low and high salt conditions were suspended in 20 mM phosphate buffer at pH 7 to make up a final biomass concentration (wet weight) of 1%

(w/v). Zeta potentials were calculated from electrophoretic mobility data using Smoluchowski's equation [28]. The small-sized particles of the chromatographic adsorbents were suitable to measure their electrophoretic mobility. All measurements were performed in triplicate. Zeta potentials at high salt concentration were extrapolated from experimentally measured values using known correlations [34].

2.6. Biomass deposition experiments

The chromatographic adsorbents (DEAE and phenyl) were thoroughly washed 3 times with water and 20 mM phosphate buffer at pH 7.5. Biomass deposition experiments were performed on an ÄKTA explorer system using a C-10 column. A 4 mL pulse of biomass that contained a known amount of yeast cells such that the OD of the pulse at 600 nm was 0.8 AU was injected into the fluidized bed column. An operational flow rate of 2 mL/min was employed in order to promote the formation of a stable expanded bed. For IEX experiments, 20 mM phosphate buffer at pH 7.5 and 1 M NaCl in the same buffer were used for binding and elution, respectively. For HIC experiments, 1 M ammonium sulfate in 20 mM phosphate buffer at pH 7.5 and the same buffer without ammonium sulfate was used for binding and elution, respectively. The biomass transmission index (CTI) was calculated from the area of the biomass pulse in the UV chromatogram before passing through the column (A_{before}) as well as after passing through the column (A_{after}) as shown in Equation 1.

$$CTI(\%) = \frac{A_{after}}{A_{before}} \times 100 \quad (1)$$

2.7. Extended DLVO calculations

The total xDLVO interaction energy (U^{XDLVO}) between two colloidal surfaces, as shown in Equation 2, is expressed as the sum of contributions from three components, namely, hydrophobic Lifshift-van der Waals (U^{LW}), polar acid-base (U^{AB}), and electrostatic (U^{EL}) interaction energies [35].

$$U^{XDLVO} = U^{LW} + U^{AB} + U^{EL} \quad (2)$$

By measuring the contact angles (θ_L) formed on an unknown surface (S) with three diagnostic liquids (whose surface energy parameters are known) one can determine the surface energy component (the hydrophobic Lifshift-van der Waals component, γ^{LW}; and polar acid-base components, γ^+ and γ^-) of the surface itself by simultaneously solving the Young-Dupré equation for each liquid (L) as shown in Equation 3 [35]. In our case, we have employed a well-established combination of probe liquids, namely, 1-bromonaphthalene (apolar), formamide (polar), and water (polar).

$$(1+\cos\theta_L)\gamma_L = 2\left(\sqrt{\gamma_S^{LW}\gamma_L^{LW}} + \sqrt{\gamma_S^{+}\gamma_L^{-}} + \sqrt{\gamma_S^{-}\gamma_L^{+}}\right) \quad (3)$$

The electrostatic interaction energy component depends not only on measured zeta potentials of the interacting surfaces, but also on the calculated Debye-Hückel length (k^{-1}) of the solution (see Equation 4), which in turn depends on the ionic strength of the medium (μ), its dielectric constant (ε_r), as well as its temperature (T).

$$\kappa^{-1} = \sqrt{\frac{\varepsilon_0 \varepsilon_k k_B T}{2 \cdot N_A e^2 \mu}} \quad (4)$$

The surface energy parameters calculated from Equation 3, as well as the zeta potentials of involved surfaces along with the Debye-Hückel length (Equation 4) are consequently used to calculate U^{LW}, U^{AB}, and U^{EL} interaction energy components using the standard equations of xDLVO theory that were adapted for biomass-adsorbent systems and which are mentioned in several previous reports [17,27,36,37].

3. Results and Discussion

3.1. Biomass cultivation and harvesting

H. polymorpha was grown as described in material methods section and Fig. 1 shows the growth characteristics at different phases. The graph plot passes through four distinctive phases, *i.e.* lag, log (early and later), stationary and death phases. It can be seen that the lag phase lasted less than 5 h before the log phases began and continued till 50 h before reaching stationary and proceeded through death phase when the medium nutrients are depleting.

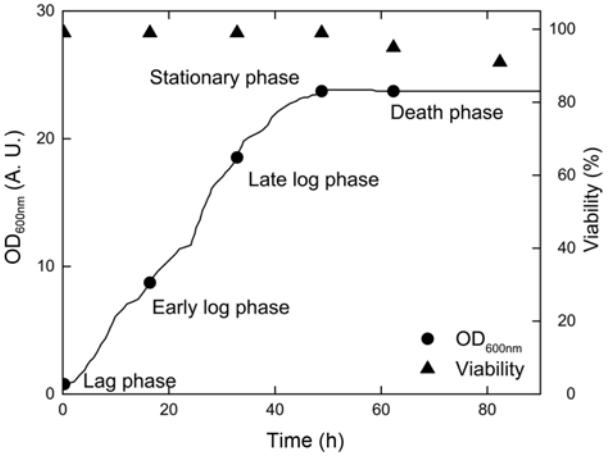

Fig. 1. Cultivation growth curve (line with dots) and cell viability (triangle) of the wild type *H. polymorpha* at different growth stages, *i.e.*, early log phase (16 h), late log phase (32 h), stationary phase (48 h), and death phase (62 h).

During these phases the change in cell viability is clearly noticed, ranging from 100% in lag to 91% in death phase (Fig. 1). For experimental analysis cells were harvested in their early log, late log, stationary as well as death phases. Additionally, disrupted cellular homogenates were prepared from cells in their late log growth phase.

3.2. Contact angle measurements

The contact angles made by the diagnostic probe liquids, namely, water, formamide, and 1-bromonaphthalene on cell in various conditions are presented in Table 1, and were used to calculate the corresponding surface energetic parameters of these cells. These probe liquids have been selected for surface characterizations due to their relatively high surface energies, and have been extensively used in the previous studies of this nature [17,31,35,38]. While the completely hydrophobic 1-bromonaphthalene characterizes the Lifshitz-van der Waals component (γ^{LW}) of the total surface energy of the biomass, the relatively polar liquids, water and formamide, characterize its acid-base components (γ^+ and γ^-) using Equation 3. These results have been summarized in Table 2, where one can observe several interesting trends. For example, the LW component increases with cell growth in low salt conditions; however, in high salt conditions, it is larger and remains approximately constant. Both acid-base energy components decrease upon cell growth in low salt conditions, and in a similar way to the LW component, remain roughly constant in high salt conditions. Furthermore, in high salt conditions, the absolute values of γ^+ are lower, whereas γ^- values are higher. In the case of disrupted cellular fragments, the LW component is slightly higher and while the γ^+ component is lower as compared to intact cells, and this combination results in a lower total surface energy in either salt condition. The above observed results can be explained on the fundamental changes occurring on the cell surface compositions during fermentation when the medium is depleted of necessary nutrients, resulting in the rearrangements of the cell wall, in terms of the hydrophobicity and adhesion. These phenomenon have also been observed in other yeasts like in nutrient-depleted *S. cerevisiae* in which specific changes to the cell at the level of the cell-wall organization, nutrient consumption, and cellular interactions with the surrounding environment occurred during different growth phases [26,29,39]. Analytically, the significance of these trends emerges in Table 3, where Lifshitz-van der Waals (ΔG^{LW}) and acid-base (ΔG^{AB}) interaction free energies of the biomass phases with different adsorbents have been calculated. In general, higher salt concentrations result in slightly higher interaction free energies. Additionally, LW free energies faintly increase with each subsequently biomass growth phase only in low salt conditions, and remain roughly constant at high salt concentrations. Acid-base free energies remain roughly the same for the different

Table 1. Contact angles of water (θ_W), formamide (θ_{FAM}), and 1-bromonaphthalene (θ_{ABN}) of intact (early log, late log, stationary, death) and disrupted (late log) biomass phases of *H. polymorpha* at low and high salt concentrations

Growth phases	θ_W		θ_{FAM}		θ_{ABN}	
	Low salt	High salt	Low salt	High salt	Low salt	High salt
Early log phase[a]	12.1 ± 0.1	13.6 ± 2.4	18.3 ± 0.7	19.7 ± 2.1	57.4 ± 1.1	50.4 ± 4.1
Late log phase[a]	14.9 ± 2.3	15.6 ± 1.7	18.9 ± 1.8	23.7 ± 2.7	56.3 ± 0.2	49.1 ± 2.2
Stationary phase[a]	19.5 ± 0.1	16.5 ± 0.3	21.2 ± 0.9	22.5 ± 1.6	53.3 ± 0.6	48.3 ± 1.1
Death phase[a]	16.9 ± 1.3	17.6 ± 0.5	18.2 ± 3.2	21.2 ± 1.8	50.3 ± 5.5	49.2 ± 1.3
Late log phase[b]	15.6 ± 0.6	24.7 ± 0.9	19.9 ± 0.8	21.7 ± 0.7	48.3 ± 3.1	45.2 ± 1.2

[a]Intact cells.
[b]Disrupted cells. Low salt conditions: 20 mM phosphate buffer at pH 7. High salt conditions: 1 M $(NH_4)_2SO_4$ in 20 mM phosphate buffer at pH 7.

Table 2. Surface energy components of intact (early log, late log, stationary, death) and disrupted (late log) biomass phases of *H. polymorpha* at low and high salt concentrations

Growth phases	γ^{LW}		γ^+		γ^-		γ^{Total}	
	LS	HS	LS	HS	LS	HS	LS	HS
Early log phase[a]	26.3	29.8	4.5	3.1	54.7	55.0	57.7	55.8
Late log phase[a]	26.8	30.4	4.3	2.6	53.5	55.4	57.1	54.4
Stationary phase[a]	28.3	30.7	3.6	2.4	51.6	55.6	55.4	53.3
Death phase[a]	29.8	30.2	3.4	2.9	52.2	53.3	56.3	55.0
Late log phase[b]	30.8	32.3	2.8	2.1	54.1	52.3	55.4	52.9

[a]Intact cells.
[b]Disrupted cells. Low salt conditions: 20 mM phosphate buffer at pH 7. High salt conditions: 1 M $(NH_4)_2SO_4$ in 20 mM phosphate buffer at pH 7.

Table 3. Calculated Lifshitz-van der Waals (ΔG^{LW}) and acid-base (ΔG^{AB}) interaction free energies of biomass phases with IEX and HIC adsorbents in different salt conditions

Growth phase	DEAE (mJ/m^2)				Phenyl (mJ/m^2)			
	Low salt		High salt		Low salt		High salt	
	ΔG^{LW}	ΔG^{AB}	ΔG_{LW}	ΔG_{AB}	ΔG_{LW}	ΔG_{AB}	ΔG_{LW}	ΔG_{AB}
Early log phase[a]	-1.1	30.2	-1.9	32.1	-1.0	29.0	-1.7	30.8
Late log phase[a]	-1.2	29.9	-2.0	33.0	-1.1	28.7	-1.8	31.6
Stationary phase[a]	-1.5	29.8	-2.0	33.3	-1.4	28.6	-1.8	32.0
Death phase[a]	-1.9	30.3	-1.9	31.5	-1.7	29.1	-1.8	30.3
Late log phase[b]	-2.0	32.0	-2.4	32.2	-1.8	30.8	-2.1	31.0

[a]Intact cells.
[b]Disrupted cells. Low salt conditions: 20 mM phosphate buffer at pH 7. High salt conditions: 1 M $(NH_4)_2SO_4$ in 20 mM phosphate buffer at pH 7.

Table 4. Zeta potentials obtained for *H. polymorpha* cells in different growth phases in different salt conditions

Growth phase	Zeta potential (mV)			
	Low salt conditions		High salt conditions	
	Intact cells	Disrupted cells	Intact cells	Disrupted cells
Early log phase	−9	-	−1.2	-
Late log phase	−10	−8	−1.3	−1.0
Stationary phase	−11	-	−1.4	-
Death phase	−12	-	−1.7	-

Low salt conditions: 20 mM phosphate buffer at pH 7. High salt conditions: 1 M $(NH_4)_2SO_4$ in 20 mM phosphate buffer at pH 7.

cell growth phases. Interestingly, interaction free energies are higher for the DEAE adsorbent as compared to the phenyl adsorbent.

3.3. Zeta potential

The component needed for determining the total interaction energy is electrostatic in nature (see Equation 2). Since the measurement of absolute surface charge is quite difficult [35], a convenient way to describe the charge characteristics of a surface is *via* its zeta potential. The cell surface energetic parameters determined earlier are mainly dependent on the inherent morphology and composition of the surface rather than the composition of its surrounding. This is evident from the relatively small absolute deviations to these parameters in different salt conditions. In contrast, the electrostatic behavior of surfaces is highly dependent on the composition of the surrounding media. It follows that zeta potentials are very sensitive to solution composition, especially ionic strength, where an increasing salt concentration results in electrostatic screening effects [35]. Furthermore, changes in solution pH, which leads to altered protonation states on the surface, also leads to changes in observed zeta potentials. These effects are observed in the measured zeta potentials for the different biomass phases (Table 4). Since microbial cell surface properties like hydrophobicity and surface charge depend on the nutritional composition medium [29], reduction in nitrogen source (starvation) induces the production of a cell-wall glycoproteins (O-mannosylated protein) [21,22,29], that become phosphorylated at different growth phases thereby giving the outer cell surface of yeast negatively charged groups [26], hence providing an anionic surface charge *i.e.* the increase in the characteristic negative charge observed in *H. polymorpha* through its growth, a similar effect observed in *Ferroplasma acidiphilum* [29]. As expected, in high salt conditions, zeta potentials are significantly reduced from up to − 12 mV to roughly the same value of ca. − 1.5 mV. The same effect is observed for disrupted cellular fragments.

3.4. Biomass deposition

Upon combining energy contributions from hydrophobic, polar, as well as electrostatic components, we have generated distance-dependent xDLVO interaction energy profiles for several biomass-adsorbent pairs in different solution conditions. These adsorbents were previously characterized by our group using methods similar to those described in this study [27,38]. In order to address these interactions in ion-exchange chromatography (IEX), we have studied the behavior of various cell growth phases with Streamline DEAE adsorbents in binding (low salt) as well as elution (high salt) conditions (Fig. 2). The most drastic variance in the secondary minima of interaction energies is observed in low salt conditions at an interfacial distance of *ca.* 5 ~ 7 nm

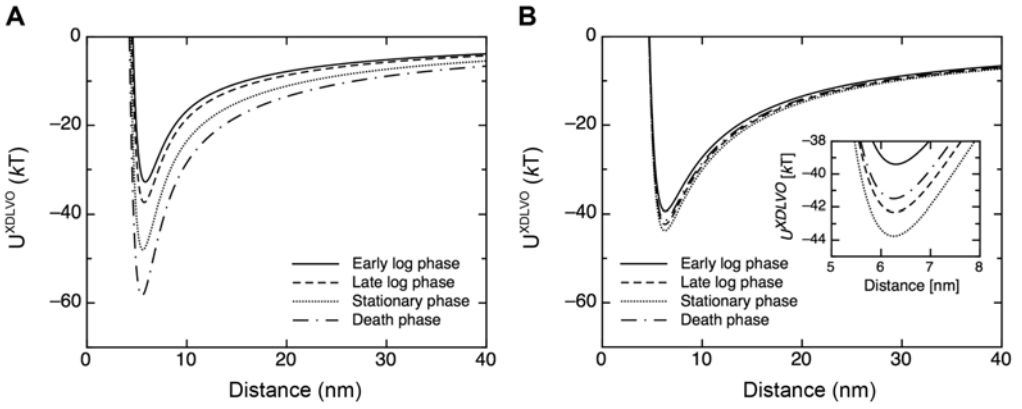

Fig. 2. xDLVO interaction energy *vs.* distance profiles of intact *H. polymorpha* cells in their early log, late log, stationary, and death phases with Streamline DEAE beads at (A) low salt/binding conditions (20 mM phosphate buffer at pH 7), and (B) high salt/elution conditions (1 M $(NH_4)_2SO_4$ in 20 mM phosphate buffer at pH 7).

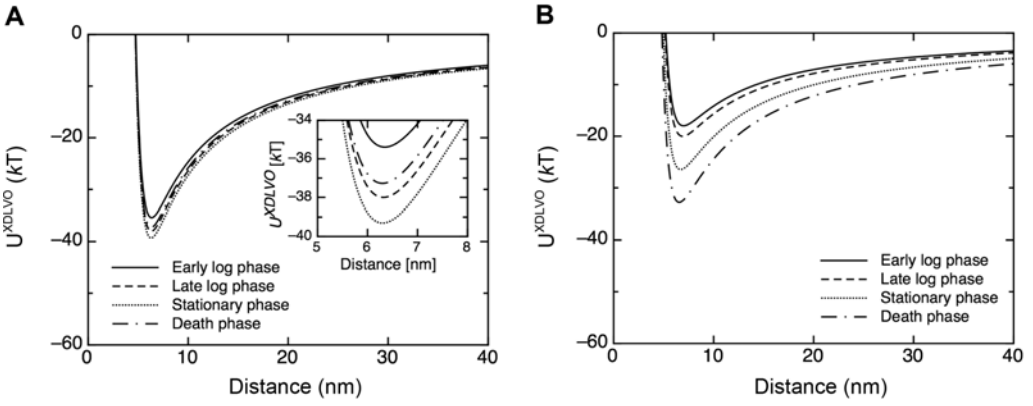

Fig. 3. xDLVO interaction energy *vs.* distance profiles of intact *H. polymorpha* cells in their early log, late log, stationary, and death phases with Streamline phenyl beads at (A) high salt/binding conditions (1 M $(NH_4)_2SO_4$ in 20 mM phosphate buffer at pH 7), and (B) low salt/elution conditions (20 mM phosphate buffer at pH 7).

(Fig. 2A). In contrast, the relative variance in secondary minima at high salt conditions is rather small (Fig. 2B). This is indicative of the strong electrostatic contributions to the total xDLVO energy in low salt conditions, while illustrating the relatively uniform behavior of all biomass phases at higher salt concentrations [40,41]. The important implication for EBA chromatography revealed by these calculations is that biomass adhesion to the DEAE adsorbent is expected to increase with each successive growth stage in low salt conditions, and as far as possible, cells in their early of late log phases are more suitable for anion-exchange EBA processes.

Complementary to ion-exchange chromatography, we probed the interaction of the same biomass phases with hydrophobic interaction chromatography (HIC) matrices using Phenyl Sepharose CL-4B adsorbents (Fig. 3). Interestingly, higher salt conditions foster larger biomass-adsorbent interactions as compared to low salt conditions, presumably due to the relatively hydrophobic nature of the adsorbent as well as an enhancement of hydrophobic and acid-base interactions in these conditions. Once again, biomass adhesion to the adsorbent is expected to increase with each successive growth stage as the *FLO* genes which encode cell-surface glycoproteins (adhesins) are activated, thereby facilitating the biofilm formation [25], however, relative differences in secondary minima of interaction energies (also at an interfacial distance of *ca.* 5 ~ 7 nm) for biomass phases are more pronounced at low salt concentrations (Fig. 3B). Therefore, since binding conditions for HIC processes require high salt concentrations, it makes little difference which growth phase of the cell is used.

Since many microbial bioproducts are intracellular, we generated interaction energy profiles for both types of adsorbents with disrupted cells in high as well as low salt conditions (Fig. 4). The small size of the disrupted biomass fragments (< 2 μm diameter) is reflected in the relatively lower interaction energies as compared to intact cells. Nevertheless, the HIC adsorbent showed a higher interaction

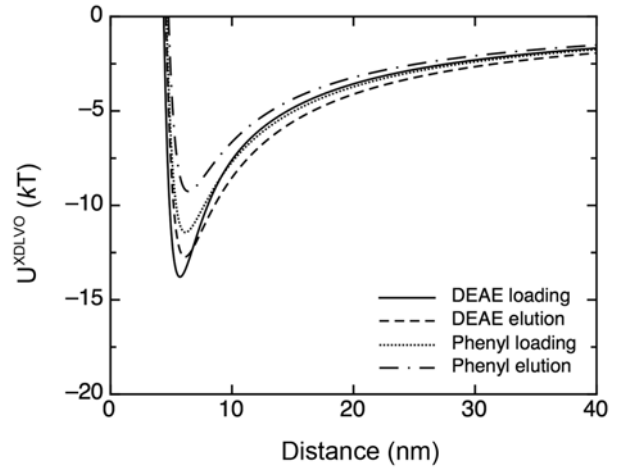

Fig. 4. xDLVO interaction energy *vs.* distance profiles of disrupted *H. polymorpha* cells in their late log phase with Streamline DEAE and Streamline phenyl beads at high salt (1 M $(NH_4)_2SO_4$ in 20 mM phosphate buffer at pH 7) and low salt conditions (20 mM phosphate buffer at pH 7).

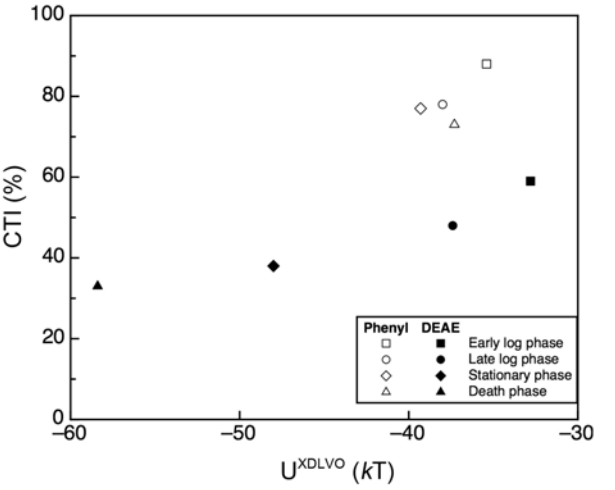

Fig. 5. Correlation between the secondary minima of total xDLVO interaction energy and the CTI of all growth phases of biomass with Streamline DEAE (solid markers) and Streamline phenyl (outlined markers).

with disrupted biomass regardless of salt concentration.

3.5. Extended DLVO

To validate the theoretical xDLVO calculations, we conducted several biomass deposition experiments to probe biomass adhesion on to adsorbents used in this study under process conditions. The cell transmission index (CTI) provides a convenient and direct measure of the fraction of cellular matter that has adhered to the adsorbent (see Equation 1). Furthermore, the CTI is measured in expanded bed mode, thereby simulating process conditions, albeit at lower flowrates (*ca.* 75 cm/h) and consequently, lower bed expansion factors (1.2 ~ 1.7) in order to more clearly demonstrate the deposition of biomass by increasing its residence time in the column [27]. Fig. 5 illustrates a general correlation between CTIs and calculated xDLVO interaction energy secondary minima of intact cells in various growth phases with Streamline DEAE and Phenyl Sepharose adsorbents at binding/loading conditions. As mentioned previously, as the cell cycle progresses, predicted interactions with the anion exchange adsorbent get stronger, and consequently, more cells adhere to the adsorbent, which is indeed what is observed in Fig. 5. We also observe less biomass adhesion for the HIC adsorbent, both *via* theoretical xDLVO calculations as well as experimental CTI values in Fig. 5. This is explained not only by reduced electrostatic biomass-adsorbent interactions, but also by concurrent interactions between cells, where calculated cell-to-cell interactions show almost twice as much cell aggregation in high salt conditions. Adhered cell aggregates, due to their significantly larger size, are more easily washed off the adsorbents as a result of hydrodynamic sheer forces [27,37], leading to higher CTIs at higher salt concentrations.

It is important to note that interactions energies between different adsorbent matrices do not quantitatively compare in terms of CTIs. Nevertheless, xDLVO calculations correctly explain the adhesion phenomena – the deeper the interaction energy pocket (Figs. 2 and 3), the greater the corresponding CTI for a biomass-adsorbent pair for the same salt condition (Fig. 5).

4. Conclusion

The results of this study employ colloid theoretical methods to trace the evolution of surface characteristics of the methylotrophic yeast, *Hansenula polymorpha*, during its different growth phases. Contact angles with diagnostic probe liquids provided information on surface thermodynamic parameters of these biomass phases, whereas zeta potential measurements characterized their surface electrostatics. Biomass-adsorbent interactions are unfavorable phenomena that adversely affect expanded bed adsorption chromatographic operations, which serve as a promising technology for the purification of biopharmaceuticals. Calculations revealed that changes in solution conditions most drastically affected electrostatic interactions, where low ionic strength conditions promote such interactions, while high ionic strength conditions screened them. They also revealed that progressive cell growth phases have an increasing interaction to anion exchange adsorbents bearing DEAE ligands in column loading conditions. Extended DLVO theory provides a versatile and pertinent framework to describe these biomass interactions, therefore, and holds

the potential of designing optimized EBA processes aimed at minimizing them in the future.

Acknowledgements

Marcelo Fernández-Lahore is member of the Consejo Nacional de Investigaciones Cientificas (CONICET) (Buenos Aires, Argentina). This work was jointly funded by the European Union Seventh Framework Programme (FP7/2007-2013) under grant agreement n°312004, as well as the DFG Project FE-3 AFM- DLVO-Theorien, Project No. 50364.

References

1. Walsh, G. (2012) A review of new biologic drug approvals over the years, featuring highlights from 2010 and 2011. *BioPharm. Int.* 25: 34-38.
2. Reichert, J. and C. Paquette (2003) Therapeutic recombinant proteins: Trends in US approvals 1982 to 2002. *Curr. Opin. Mol. Ther*. 5: 139-147.
3. Anspach, F. B., D. Curbelo, R. Hartmann, G. Garke, and W. -D. Deckwer (1999) Expanded-bed chromatography in primary protein purification. *J. Chromatogr. A*. 865: 129-144.
4. Wheelwright, S. M. (1991) *Protein Purification: Design and Scale Up of Downstream Processing*. Hanser Publishers.
5. Harrison, R. G., P. Todd, S. R. Rudge, and D. P. Petrides (2003) *Bioseparations Science and Engineering*. Oxford University Press, NY.
6. D'Souza, R. N., A. M. Azevedo, M. R. Aires-Barros, N. L. Krajnc, P. Kramberger, M. L. Carbajal, M. Grasselli, R. Meyer, and M. Fernández-Lahore (2013) Emerging technologies for the integration and intensification of downstream bioprocesses. *Pharm. Bioproc.* 1: 423-440.
7. Chase, H. A. (1994) Purification of proteins by adsorption chromatography in expanded beds. *Trends Biotechnol.* 12: 296-303.
8. Feuser, J., J. Walter, M. -R. Kula, and J. Thömmes (1999) Cell/adsorbent interactions in expanded bed adsorption of proteins. *Bioseparation* 8: 99-109.
9. Barnfield Frej, A. -K., R. Hjorth, and Å. Hammarström (1994) Pilot scale recovery of recombinant annexin V from unclarified *Escherichia coli* homogenate using expanded bed adsorption. *Biotechnol. Bioeng.* 44: 922-929.
10. Calado, C. R. C., J. M. S. Cabral, and L. P. Fonseca (2002) Effect of Saccharomyces cerevisiae fermentation conditions on expanded bed adsorption of heterologous cutinase. *J. Chem. Technol. Biotechnol.* 77: 1231-1237.
11. Beck, J. T., B. Williamson, and B. Tipton (1999) Direct coupling of expanded bed adsorption with a downstream purification step. *Bioseparation* 8: 201-207.
12. Blank, G. S., G. Zapata, R. Fahrner, M. Milton, C. Yedinak, H. Knudsen, and C. Schmelzer (2001) Expanded bed adsorption in the purification of monoclonal antibodies: A comparison of process alternatives. *Bioseparation* 10: 65-71.
13. Timo May, K. P. (2011) Improving process economy with expanded-bed adsorption technology. *Bioproc. Int.* 9: 32-36.
14. Walter, J. K. and J. Feuser (2003) Novel approach and technology in expanded bed adsorption techniques for primary recovery of proteins at large technical scale. *Proceedings of the Extended reports from the 4th International Conference on Expanded Bed Adsorption*.
15. Lin, D. Q., H. M. Fernandez-Lahore, M. R. Kula, and J. Thommes (2001) Minimising biomass/adsorbent interactions in expanded bed adsorption processes: A methodological design approach. *Bioseparation*. 10: 7-19.
16. Fernández-Lahore, H. M., R. Kleef, M. R. Kula, and J. Thömmes (1999) The influence of complex biological feedstock on the fluidization and bed stability in expanded bed adsorption. *Biotechnol. Bioeng.* 64: 484-496.
17. Vennapusa, R., S. M. Hunegnaw, R. B. Cabrera, and M. Fernandez-Lahore (2008) Assessing adsorbent-biomass interactions during expanded bed adsorption onto ion exchangers utilizing surface energetics. *J. Chromatogr. A.* 1181: 9-20.
18. Fernández-Lahore, H. M., S. Geilenkirchen, K. Boldt, A. Nagel, M. R. Kula, and J. Thömmes (2000) The influence of cell adsorbent interactions on protein adsorption in expanded beds. *J. Chromatogr. A*. 873: 195-208.
19. Poulin, F., R. Jacquemart, G. de Crescenzo, M. Jolicoeur, and R. Legros (2008) A study of the interaction of HEK-293 cells with streamline chelating adsorbent in expanded bed operation. *Biotechnol. Progr.* 24: 279-282.
20. Smith, M. P., M. A. Bulmer, R. Hjorth, and N. J. Titchener-Hooker (2002) Hydrophobic interaction ligand selection and scale-up of an expanded bed separation of an intracellular enzyme from Saccharomyces cerevisiae. *J. Chromatogr. A*. 968: 121-128.
21. Skvarla, J. (1993) A physicochemical model of microbial adhesion. *J. Chem. Soc. Faraday Tran*. 89: 2913-2921.
22. Kondo, A., and M. Ueda (2004) Yeast cell-surface display - applications of molecular display. *Appl. Microbiol. Biot*. 64: 28-40.
23. Ravin, N. V., M. A. Eldarov, V. V. Kadnikov, A. V. Beletsky, J. Schneider, E. S. Mardanova, E. M. Smekalova, M. I. Zvereva, O. A. Dontsova, A. V. Mardanov, and K. G. Skryabin (2013) Genome sequence and analysis of methylotrophic yeast Hansenula polymorpha DL1. *BMC Genomics*. 14: 837.
24. Ma, Y., M. Zhou, S. Walter, J. Liang, Z. Chen, and L. Wu (2014) Selective adhesion and controlled activity of yeast cells on honeycomb-patterned polymer films *via* a microemulsion approach. *Chem. Commun.*50: 15882-15885.
25. Kurec, M., and T. Branyik (2011) The role of physicochemical interactions and FLO genes expression in the immobilization of industrially important yeasts by adhesion. *Colloids Surf., B*. 84: 491-497.
26. Bou Zeidan, M., G. Zara, C. Viti, F. Decorosi, I. Mannazzu, M. Budroni, L. Giovannetti, and S. Zara (2014) L-histidine inhibits biofilm formation and FLO11-associated phenotypes in *Saccharomyces cerevisiae* flor yeasts. *PloS one*. 9: e112141.
27. Vennapusa, R. R., C. Tari, R. Cabrera, and M. Fernandez-Lahore (2009) Surface energetics to assess biomass attachment onto hydrophobic interaction adsorbents in expanded beds. *Biochem. Eng. J.* 43: 16-26.
28. Ottewill, R. H. and J. N. Shaw (1972) Electrophoretic studies on polystyrene latices. *J. Electroanal. Chem. Interfacial Electrochem*. 37: 133-142.
29. Farahat, M. and T. Hirajima (2012) Hydrophilicity of Ferroplasma acidiphilum and its effect on the depression of pyrite. *Miner. Eng*. 36-38: 242-247.
30 . Lipke, P. N. and J. Kurjan (1992) Sexual agglutination in budding yeasts: Structure, function, and regulation of adhesion glycoproteins. *Microbiol. Rev.* 56: 180-194.
31. Tari, C., R. Vennapusa, R. B. Cabrera, and M. Fernández-Lahore (2008) Colloid deposition experiments as a diagnostic tool for biomass attachment onto bioproduct adsorbent surfaces. *J. Chem. Technol. Biotechnol.* 83: 183-191.
32. Kucsera, J., K. Yarita, and K. Takeo (2000) Simple detection

method for distinguishing dead and living yeast colonies. *J. Microbiol. Methods*. 41: 19-21.
33. Sharma, P. K. and K. Hanumantha Rao (2002) Analysis of different approaches for evaluation of surface energy of microbial cells by contact angle goniometry. *Adv. Colloid. Interface Sci.* 98: 341-463.
34. Huang, A. Y. and J. C. Berg (2006) High-salt stabilization of Laponite clay particles. *J. Colloid. Interface Sci.* 296: 159-164.
35. van Oss, C. J. (2006) *Interfacial Forces in Aqueous Media*. 2nd ed. Taylor & Francis, Boca Raton.
36. Vennapusa, R. R., M. Aasim, R. Cabrera, and M. Fernandez-Lahore (2009) Surface energetics to assess biomass attachment onto immobilized metal-ion chromatography adsorbents in expanded beds. *Biotechnol. Bioproc. Eng*. 14: 419-428.
37. Vennapusa, R. R., O. Aguilar, J. M. B. Mintong, G. Helms, J. Fritz, and M. F. Lahore (2010) Biomass-adsorbent adhesion forces as an useful indicator of performance in expanded beds. *Separ. Sci. Technol*. 45: 2235-2244.
38. Vennapusa, R. R., S. Binner, R. Cabrera, and M. Fernandez-Lahore (2008) Surface energetics to assess microbial adhesion onto fluidized chromatography adsorbents. *Eng. Life Sci.* 8: 530-539.
39. Farahat, M., T. Hirajima, K. Sasaki, and K. Doi (2009) Adhesion of *Escherichia coli* onto quartz, hematite and corundum: Extended DLVO theory and flotation behavior. *Colloids Surf. B*. 74: 140-149.
40. Lin, D. -Q., P. J. Brixius, J. J. Hubbuch, J. Thömmes, and M. -R. Kula (2003) Biomass/adsorbent electrostatic interactions in expanded bed adsorption: A zeta potential study. *Biotechnol. Bioeng.* 83: 149-157.
41. Lin, D. -Q., L. -N. Zhong, and S. -J. Yao (2006) Zeta potential as a diagnostic tool to evaluate the biomass electrostatic adhesion during ion-exchange expanded bed application. *Biotechnol. Bioeng.* 95: 185-191.